Generating Switchable Structural Colors in the Visible Range Using Phase-Change Materials

Ramón Camilo Domínguez Ordóñez
S6019234*

Science and Engineering Department,
Nanoscience,
NL-9700 AE Groningen
The Netherlands

(April 13, 2025)

Phase-change materials (PCMs) have emerged as versatile platforms for reconfigurable photonics as a result of their tunable optical properties in amorphous and crystalline states. This review focuses on their application in generating switchable structural color in the visible spectrum, highlighting how abrupt changes in refractive index and absorption enable active control of interference-based coloration. We examine the optical behavior of widely studied PCMs, such as $Ge_2Sb_2Te_5$ (GST), VO_2, Sb_2S_3, and Sb_2Se_3, and assess their performance in terms of index contrast, optical loss, and spectral coverage. Switching mechanisms, including thermal, electrical, and all-optical actuation, are compared in the context of dynamic modulation and device integration. Finally, we present recent experimental demonstrations of structural color generation, ranging from multilayer interference stacks to nanoscale FIB-patterned metasurfaces, with particular emphasis on wide-bandgap PCMs that enable high-resolution, low-loss color rendering. We conclude by describing key challenges related to scalability, endurance, and addressability, and highlight future directions toward fully reconfigurable nanostructured photonic systems.

CONTENTS

I. INTRODUCTION

The study of color dates back centuries. Isaac Newton's 1666 work with prisms revealed that white light splits into a continuous spectrum of colors. Although Newton focused on absorption and transmission, later research identified structural color, where periodic nanoscale structures manipulate light through interference, diffraction, or scattering rather than relying on molecular absorption (Nassau, 1987). This mechanism explains the vibrant iridescence of butterfly wings, peacock feathers, and opals and has become a key focus in photonics and display technologies (Ko *et al.*, 2022).

Ancient artifacts provided early evidence of nanostructured optical effects. One of the earliest known examples is the Lycurgus cup, an ancient Roman artifact that exhibits a striking color shift between red and green depending on the light source and viewing angle. This effect results from the plasmonic resonance caused by the gold and silver nanoparticles embedded in the glass (Freestone *et al.*, 2007). Later advances in optics and material science during the mid-20th century provided new ways to manipulate light at subwavelength scales. In 1947, Dennis Gabor developed holography, introducing a method to capture and reconstruct optical wavefronts, which later was used in applications in three-dimensional imaging and data storage (Gabor, 1972). Around the same time, research into photonic crystals revealed their ability to create photonic band gaps, controlling light propagation. At the same time, plasmonic nanostructures and metasurfaces allowed fine-tuning of reflection, absorption, and scattering (Fang *et al.*, 2020; Han *et al.*, 2019; Ren *et al.*, 2020; Wuttig *et al.*, 2017). These breakthroughs have led to tunable photonic systems, where structural color

* R.C.Dominguez.Ordonez@student.rug.nl

can be dynamically adjusted for applications in imaging, adaptive optics, and reconfigurable displays (Ozbay, 2006; Yu *et al.*, 2014; Zhang *et al.*, 2019).

In 1959, Richard Feynman introduced the idea of manipulating matter at the atomic scale in his lecture "There is Plenty of Room at the Bottom," a concept that later became fundamental to the development of nanoscience (Feynman, 1960). This vision is directly relevant to structural color research, where nanoscale control enables the tuning of optical properties beyond what is achievable with traditional pigments. Nassau *et* al. classified color generation mechanisms into five main categories: (i) vibrations and excitations, (ii) ligand field effects, (iii) molecular orbital transitions, (iv) energy bands and (v) geometrical and physical optics. Structural color falls into the last group, governed by interference, diffraction, and scattering phenomena responsible for the vivid colors seen in natural and engineered systems (Nassau, 1987).

The interaction between light and matter is central to all optical phenomena. Since Dirac and Fermi laid the groundwork for quantum electrodynamics (Dirac and Bohr, 1927; Fermi, 1932), it has been understood that light can behave both as a wave and as photons coupling with material excitations such as plasmons, phonons, and excitons (Rivera and Kaminer, 2020). Light can also be transmitted, reflected, absorbed, refracted, polarized, diffracted, or scattered in engineered nanostructures depending on the geometry and composition of the material and the wavelength of the light, which directly affects perceived color (Ko *et al.*, 2022). Metasurfaces and plasmonic arrays apply these effects to control the optical behavior at the nanoscale (Rivera and Kaminer, 2020). Research on photonic crystals and resonant nanostructures has made it possible to control visible light at scales below the diffraction limit, with practical use in thin film coatings, optical routing, and light modulation (Selvaraja *et al.*, 2018). However, most of these structures remain fixed after fabrication, which limits their integration into systems requiring tunable or reprogrammable responses.

Structural color results from nanoscale structures that alter light through interference, diffraction, and plasmonic resonance (Nassau, 1987). In thin films, variations in optical path length between interfaces produce angle-dependent color shifts, as seen in soap bubbles and oil films. Periodic nanostructures, such as photonic crystals and gratings, diffract light by wavelength, while metallic nanostructures support plasmon resonances that enhance selective absorption and scattering (Carrillo *et al.*, 2019; Ko *et al.*, 2022). Techniques such as electron beam lithography and focused ion beam milling allow fine-tuned fabrication of nanoscale features, enabling the practical use of structural coloration in areas such as optical imaging, anticounterfeiting, and bioinspired coatings (Ríos *et al.*, 2016; Yimam *et al.*, 2024). However, once fabricated, the optical behavior of these systems generally cannot be altered. Phase-change materials (PCMs) have been investigated as an alternative, as their phase transitions between amorphous and crystalline states result in marked variations in the optical properties (Wuttig *et al.*, 2017).

Phase-change materials are key for achieving tunable structural color because of their reversible changes in optical properties. Germanium-antimony-tellurium (GST) (Ding *et al.*, 2019; Hosseini *et al.*, 2014; Wuttig *et al.*, 2017) and antimony selenide (Sb_2Se_3) (Dong *et al.*, 2019; Yimam *et al.*, 2024) are two widely studied chalcogenide alloys. These materials show reversible phase transitions that change the real and imaginary components of the complex refractive index (Cao and Cen, 2019). Their ability to rapidly switch, maintain long-term stability, and withstand repeated cycles makes them suitable for optical and resistive memory devices (Abdollahramezani *et al.*, 2020). In GST, crystallization occurs around $160°C$, while re-amorphization is achieved by heating above $600°C$ (Ko *et al.*, 2022). During this transition, the refractive index drops (Δn $\approx$ -1.5 at 405 nm) and the absorption increases, shifting the reflected color toward shorter wavelengths (Abdollahramezani *et al.*, 2020; Ríos *et al.*, 2016). However, strong absorption in the visible range causes optical losses and limits efficiency. Alloys such as Ge-Sb-Se-Te (GSST), offer lower absorption and broader transparency windows (Dong *et al.*, 2019). Researchers have also investigated antimony sulfide (Sb_2S_3) and antimony selenide Sb_2Se_3 for its wide band gap and reduced absorption in the visible spectrum (Dong *et al.*, 2019). Its stable structure and strong refractive index contrast make it a strong candidate for use in tunable optical coatings and display technologies (Yimam *et al.*, 2024).

PCMs can be switched using thermal, optical, or electrical inputs. Techniques include laser pulses (Cheng *et al.*, 2021; Liu *et al.*, 2020; Raeis-Hosseini and Rho, 2017; Sun *et al.*, 2017), voltage-driven switching (Hosseini *et al.*, 2014; Sreekanth *et al.*, 2021; Wang *et al.*, 2020), and ion-beam exposure (Hafermann *et al.*, 2018). Electrical switching is particularly useful in integrated photonic systems because it allows for discrete modulation of optical states without needing constant power input. This approach has been successfully used on platforms such as metasurfaces, Fabry–Pérot resonators, and plasmonic gratings for dynamic color control (Carrillo *et al.*, 2019; Ríos *et al.*, 2016). Furthermore, partial crystallization creates intermediate states that allow one to gradually adjust the reflectance, rather than just switching between two fixed levels (Ríos *et al.*, 2016).

This review focuses on the role of phase-change materials in achieving dynamically tunable structural color, particularly within the visible spectrum. It explores how specific chalcogenide compounds alter optical constants during phase transitions and how these changes have been harnessed in nanostructured devices. We also discuss practical design challenges, material limitations, and

recent efforts to improve performance and integration in real-world systems.

II. OPTICAL PROPERTIES OF PHASE CHANGE MATERIALS

Phase-change materials (PCMs) such as Ge-Sb-Te alloys stand out from conventional solids because of their fundamentally distinct bonding mechanisms across phase states. Unlike SiO_2, which maintains similar optical behavior in both phases due to consistent covalent bonding, GST alloys exhibit sharp differences in optical response as they switch from covalent to metavalent bonding (Zhu *et al.*, 2018). In the crystalline phase, this bonding mechanism increases the electronic polarizability and significantly alters the dielectric function (Ding *et al.*, 2019).

As shown in Figure 1 **a)**, GST-225 and GST-326, among the compositions that are the most widely used, lie along the pseudo-binary $GeTe-Sb_2-Te_3$ link (Ding *et al.*, 2019). Compositions such as $GST-225$ and $GST-326$ are widely used in optical storage and metasurfaces for their reliable switching and strong optical contrast (Wuttig and Yamada, 2007; Yamada *et al.*, 1987). However, even small changes in stoichiometry can lead to noticeable changes in optical behavior (Lencer *et al.*, 2008; Raoux *et al.*, 2014).

Figure 1 **b)** shows that the phase transition of GST-225 begins in the amorphous phase, where the atoms lack long-range order. The structure becomes more ordered upon crystallization after exposure to an external stimulus (i.e., thermal, electrical, or optical), but retains vacancies, introducing free carriers that affect optical absorption and reflectance (Michel *et al.*, 2017). Although crystallization is generally thermally induced and experimentally accessible, reversing to the amorphous phase typically requires high-intensity, short-duration pulses and precise thermal quenching (>10 K/ns) (Wuttig *et al.*, 2017), often requiring additional buffer layers such as Si_3N_4 or TiN to prevent interdiffusion (Lu *et al.*, 2019).

Figure 1 **c)** presents the complex dielectric functions ϵ_1 and ϵ_2 for GST-225 in both amorphous and crystalline states (Ding *et al.*, 2019). The contrast between these phases, observed in the changes of both components ($\Delta\epsilon_1$ and $\Delta\epsilon_2$) of the dielectric function, extends across nearly the entire spectral range. A low-loss spectral window emerges in the amorphous phase below the bandgap ($\sim$ 0.7 eV), where interband transitions are absent. Meanwhile, free carriers from vacancies in the crystalline state lead to finite absorption. In the visible spectrum, c-GST shows negative values of ϵ_1, a behavior usually seen in plasmonic metals (Raoux *et al.*, 2014). This dielectric-to-plasmonic transition supports applications such as tunable photonic systems, including dynamic color filters and reconfigurable window technologies (Gholipour *et al.*, 2018). Although GST-225 is widely used, other compositions, such as GST-326 or Se-doped variants, have shown better contrast and lower losses in the mid-IR range (Michel *et al.*, 2017; Raoux *et al.*, 2014; Zhang *et al.*, 2019).

Figures 1 **d)** and **e)** compare the refractive index N and the extinction coefficient K for GeTe, $Ge_2Sb_2Te_5$ and $GeSb_2Te_4$ in the amorphous and crystalline states (Wuttig *et al.*, 2017). Crystallization leads to a substantial increase in N, especially below the band gap, most notably in the infrared region below 1 eV, where interband transitions are inactive. For some PCMs, this increase exceeds 50%, a behavior absent in conventional semiconductors such as InSb and $AgInTe_2$. This behavior cannot be explained by the density changes alone but instead stems from resonant bonding in the crystalline phase, which enhances the electronic polarizability and results in a large high-frequency dielectric constant ϵ_∞ (Lencer *et al.*, 2008; Lucovsky and White, 1973; Shportko *et al.*, 2008; Wuttig *et al.*, 2017). Above the bandgap, the optical constants still differ, although both phases become more absorptive. The contrast persists well into the infrared, making PCMs highly suitable for broadband photonic and optoelectronic applications, such as tunable optical modulators and reconfigurable IR filters (Wuttig and Yamada, 2007).

Figures 1 **f)** to **i)** present optical data for Sb_2S_3 and $Ge_2Sb_2Te_5$ (GST), highlighting key differences that make Sb_2S_3 a promising candidate for visible range photonics (Dong *et al.*, 2019). Sb_2S_3 shows a larger band gap than GST, with a redshift on its absorption edge from 2.05 eV (amorphous) to 1.72 eV (crystalline), allowing visible-light operation with significantly reduced losses (Arun and Vedeshwar, 1997). This wide band gap results in a near-zero extinction coefficient (k) in both phases across large portions of the visible range (400-900 nm), unlike GST, which remains highly absorbing (Lee *et al.*, 2005). The refractive index change ($\Delta n \approx 1$ at 614 nm) is substantial, offering strong tunability without introducing high absorption (Dong *et al.*, 2019).

Figure 1 **f)** uses a radar plot to benchmark Sb_2S_3 against GST and VO_2 in several performance indicators, including Δn, band gap, extinction coefficient, and switching time. Sb_2S_3 demonstrates a favorable balance—combining fast, nonvolatile switching ($\sim$70 ns) with broadband transparency and high refractive index modulation. Compared to VO_2 which requires constant energy to maintain its phase, and GST that suffers from high absorption in the visible range, Sb_2S_3 combines high optical contrast with low losses, making it a promising candidate for reprogrammable visible photonics (Massalski *et al.*, 1986; Tominaga *et al.*, 2009).

Figures 2 **a)** to **d)** explore how ultrathin phase change films enable reflectance control and dynamic color tunability in the visible spectrum (Hosseini *et al.*, 2014). In this architecture, a GST layer is embedded between two ITO electrodes and placed on a reflective Pt backplane.

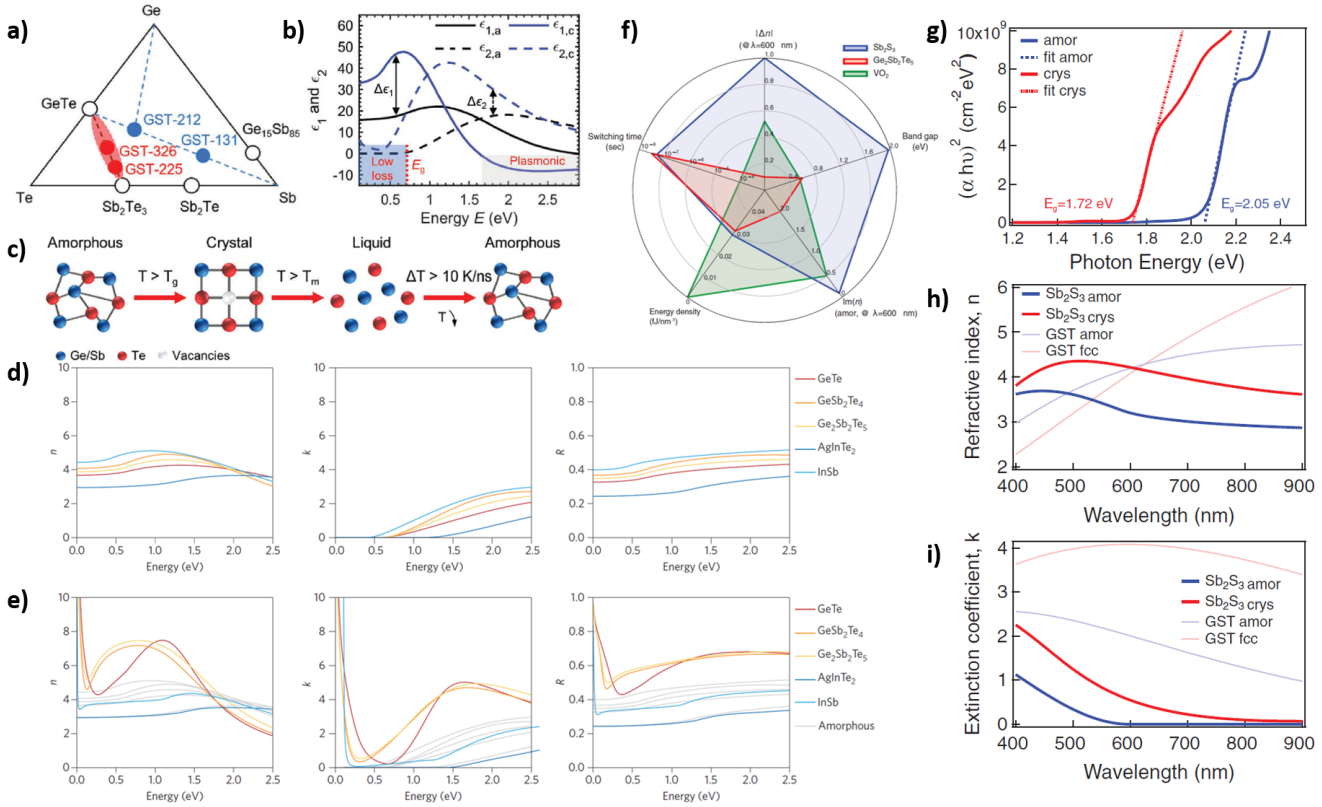

FIG. 1: **Comparison of optical properties for phase-change materials (PCMs) relevant to tunable photonics. a)** Ternary Ge-Sb-Te phase diagram showing common compositions including GST-225 and GST-326, adapted from (Ding *et al.*, 2019), originally based on data from (Lencer *et al.*, 2008). **b)** Complex dielectric functions ϵ_1 and ϵ_2 of GST-225 in amorphous and crystalline states, adapted from (Ding *et al.*, 2019), using data from (Shportko *et al.*, 2008). Shaded regions indicate low-loss (blue) and plasmonic (gray) regimes. **c)** Schematic illustration of GST thermal switching dynamics, adapted from (Ding *et al.*, 2019). **d, e)** Refractive index, extinction coefficient, and reflectance for GeTe, $Ge_2Sb_2Te_5$, and $GeSb_2Te_4$ (PCMs), compared to conventional semiconductors $AgInTe_2$ and InSb, in the amorphous **(d)** and crystalline **(e)** states, adapted from (Wuttig *et al.*, 2017). **f)** Radar plot comparing Sb_2S_3, GST, and VO_2 in terms of Δn, bandgap, absorption, switching time, and energy density at 600 nm, adapted from (Dong *et al.*, 2019). **g)** Tauc plot showing a bandgap redshift in Sb_2S_3 from 2.05 eV (amorphous) to 1.72 eV (crystalline), adapted from (Dong *et al.*, 2019). **h, i))** Real (n) and imaginary (k) parts of the refractive index for Sb_2S_3 and GST in both phases, highlighting the low-loss and high-contrast response of Sb_2S_3 in the visible, adapted from (Dong *et al.*, 2019).

The phase transition alters the refractive index of GST, leading to a measurable shift in the reflectance spectrum through interference with the ITO spacer. As shown in Figure 2 **b)**, simulated and measured reflectivity spectra for both phases show strong agreement, confirming that a GST film of a few nanometers thick can induce pronounced color changes throughout the visible range. In particular, thinner GST layers show stronger contrast, with reflectance changes exceeding 300% depending on the thickness of the ITO spacer (Figure 2 **c)**) (Hosseini *et al.*, 2014). This effect results from phase-dependent interference that boosts reflection in selected parts of the spectrum. For example, ITO spacer thicknesses of 70 nm, 150 nm, and 180 nm boost reflectivity in the blue, green, and red regions, respectively. The color switching capability is visually confirmed in Figure 2 **d)**, where films exhibit distinct hue changes upon crystallization. These results highlight the potential for the use of sub-wavelength GST pixels in reconfigurable displays and metasurfaces, supported by electrical switching and high spatial resolution (Burkhard *et al.*, 2010; Hosseini *et al.*, 2014).

Figures 2 **j)** and **k)** demonstrate how the absorption properties of Sb_2S_3 enable dynamic control of the resonant behavior in ultrathin photonic structures (Dong *et al.*, 2019). A 21 nm Sb_2S_3 film deposited on a reflective substrate exhibits perfect absorption at λ=472 nm in the amorphous state, which red-shifts to 565 nm upon crystallization. This shift is primarily driven by changes in the absorption coefficient, as the variation in the real part of the refractive index is relatively minor ($\Delta Re(n) \approx 0.3$).

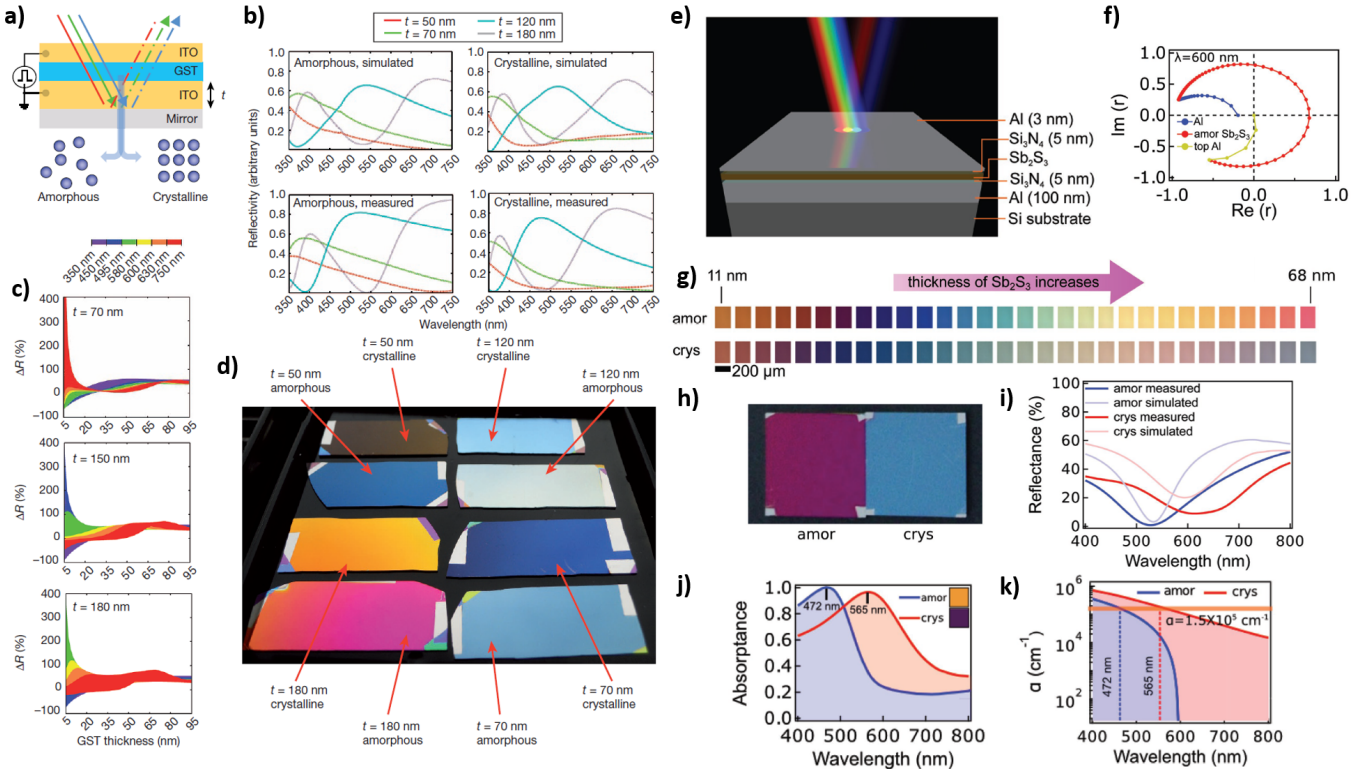

FIG. 2: **Visible-range reflectance control and color tuning using ultrathin PCMs. a)** Schematic of a reflective multilayer device consisting of ITO/GST/ITO on a metallic mirror, where phase-change-induced refractive index variations modulate the optical path. **b)** Simulated and measured reflectivity spectra of amorphous and crystalline GST-based stacks for various ITO spacer thicknesses, demonstrating phase-dependent spectral tunability. **c)** Calculated percentage reflectance change (ΔR) for different GST and ITO thicknesses, showing amplification of contrast in thinner films. **d)** Optical micrographs of fabricated devices illustrating color variation across samples before and after crystallization. **e)** Schematic of a multilayer resonator incorporating Sb_2S_3 between Al and Si_3N_4 layers, designed for tunable absorption in the visible. **f)** Complex-plane reflection coefficient of the Sb_2S_3 resonator at $\lambda = 600$ nm, illustrating changes in amplitude and phase across interfaces. **g)** Optical color response as a function of Sb_2S_3 thickness and phase, with visible chromatic shifts across the 425-710 nm range. **h)** Photographs of 24 nm-thick Sb_2S_3 samples showing the visual change in reflectance between amorphous and crystalline states. **i)** Simulated and measured reflectance spectra for amorphous and crystalline states, confirming the tunable behavior. **j)** Absorbance spectra of 21 nm Sb_2S_3 thin films showing red-shift of the resonance from 472 to 565 nm upon crystallization. **k)** Absorption coefficient (α) as a function of wavelength, indicating that switching is primarily driven by changes in the imaginary refractive index. **a-d)** adapted from (Hosseini *et al.*, 2014); **e-k)** adapted from (Dong *et al.*, 2019).

Instead, strong modulation arises from the red-shifted absorption edge and the resulting change in the imaginary refractive index, which dominates the interference condition within the sub-wavelength multilayer (Dong *et al.*, 2019). This behavior shows how wide-bandgap PCMs such as Sb_2S_3 can support strong optical contrast in the visible, not through resonant bonding like GST, but via phase-induced changes in absorption-driven interference (Dong *et al.*, 2019; Kats *et al.*, 2013).

Figures 2 **e)** to **i)** present how structural and optical modulation in Sb_2S_3-based resonators enables spectral control in the visible range through thickness-dependent design (Dong *et al.*, 2019). In Figure 2 **e)**, a multilayer stack composed of Al/Si_3N_4/Sb_2S_3/Si_3N_4/Al is used, where Si_3N_4 acts as a diffusion barrier, and the thin layer of Al improves the Q factor and allows electrical switching. The resonant condition is tuned by varying the thickness of Sb_2S_3 between 11 and 68 nm, resulting in a red shift of the reflectance peak from 425 to 710 nm (Figure 2 **g)**). The resulting color change is visible in Figure 2 **h)**, which compares the amorphous and crystalline states and is quantitatively supported by the measured and simulated reflectance spectra in Figure 2 **i)**.

The observed red-shift arises primarily from a narrowing of the band gap upon crystallization: from 2.0 to 1.7 eV and a significant increase in the imaginary part of the

refractive index, from 0.08 to 0.83 at 550 nm. Although the change in real refractive index ($\Delta Re(n) \approx 0.9$) results in only a small optical path length variation ($\sim$32 nm), the sharp absorption-edge modulation strongly affects the resonance condition. This effect is captured in the complex reflection coefficient map in Figure 2 **f)**, which shows a shift in phase and amplitude of the reflected wave at $\lambda = 600nm$.

These results highlight that, unlike GeTe–Sb_2Te_3-based PCMs where optical contrast is dominated by resonant bonding and delocalized electrons, Sb_2S_3 achieves tunability through density-driven absorption changes. Upon crystallization, the density increases by $\sim$35%, and the refractive index below the bandgap rises by $\sim$33%, well described by the Clausius-Mossotti relation (Dong *et al.*, 2019; Ghosh and Varma, 1979). This mechanism enables broadband, reconfigurable color tuning in the visible range, with potential for laser and electrically driven switching at speeds comparable to GST (Behera *et al.*, 2017; Dong *et al.*, 2019; Wuttig and Yamada, 2007).

A. Outlook and Perspectives

Visible-range photonics demands materials with both strong tunability and low absorption. Ge–Sb–Te alloys provide high optical contrast through resonant bonding, but their use in the visible range is restricted by free carrier absorption in the crystalline phase (Ding *et al.*, 2019; Wuttig *et al.*, 2017). This behavior, highlighted in the extinction coefficient spectra of Figure 1e, originates from vacancies acting as sources of intraband transitions, which dominate losses in the red and near-infrared.

In contrast, PCMs based on sulfide and selenide such as Sb_2S_3 and Sb_2Se_3 combine high refractive index modulation with minimal absorption in the visible. Dong et al. show that Sb_2S_3 maintains extinction coefficients close to zero across large portions of the visible spectrum while still achieving $\Delta n \approx 1$ at 614 nm (Dong *et al.*, 2019). Yimam *et al.*. report that Sb_2Se_3, with its wide band gap and compatibility with FIB milling, enables structural color tuning at the nanoscale (Yimam *et al.*, 2024). Both materials operate via shifts in the polarizability and absorption edges without the free-carrier losses seen in tellurides.

Although GST-based multilayers have demonstrated color modulation via phase-induced interference (Hosseini *et al.*, 2014), their tunable range is limited by absorption losses. In contrast, the stacks incorporating Sb_2S_3 shown in Figures 2e-k achieve spectral control through crystallization-driven changes in the absorption edge, with limited reliance on refractive index variation. This enables visible-range tunability with thinner films and higher reflectance contrast.

Despite these advantages, widebandgap PCMs lack comprehensive datasets across different deposition methods, and few studies compare their optical response under repeated switching. Endurance, switching energy, and stability under ambient conditions remain critical gaps for materials such as Sb_2Se_3. Integration into addressable, low-power photonic systems will also require tighter control over thickness and phase purity at the nanoscale.

Future design strategies should focus on achieving large Δn with low k in the visible spectrum while leveraging mechanisms beyond bonding transitions. Hybrid tuning schemes, which combine interference, absorption edge control, and nanoscale patterning, offer a path toward high-efficiency, programmable optics. Materials such as Sb_2S_3 and Sb_2Se_3 are strong candidates for this direction, combining optical contrast, processability, and compatibility with thin-film nanofabrication.

III. SWITCHING MECHANISMS AND OPTICAL MODULATION

A. Thermal switching

Thermal switching in phase-change materials relies on externally induced temperature changes to trigger reversible transitions between the amorphous and crystalline states; unlike electrical switching, which requires localized Joule heating, thermal approaches typically use uniform substrate heating or pulsed laser exposure, methods that are electrode-free and well suited for large-area or planar systems. Although the optical implications of this transition in GST-225 have already been addressed in the context of dielectric contrast (see Figures 1**b-c** and Section II) (Ding *et al.*, 2019), these phase changes are fundamentally rooted in temperature-driven atomic rearrangements. Heating above the glass transition temperature (T_g) enables crystallization, while melt quenching from above T_m restores the amorphous state. These processes define thermal switching as a reliable and contactless method for tuning optical properties through structural reconfiguration.

Beyond GST, the thermal switching behavior of wideband-gap PCMs such as Sb_2S_3 offers a complementary perspective rooted in the analysis of the energy landscape. As shown in Figure 1 **g-i** and Figure 2 **e-k**, Dong *et al.* illustrate the 2.0 eV activation barrier that governs the crystallization of Sb_2S_3 (Dong *et al.*, 2019; Kolobov *et al.*, 2004). Although we previously discussed the optical advantages of Sb_2S_3 in terms of refractive index contrast and low visible absorption, its thermal behavior also reflects high stability at room temperature and sharply defined switching thresholds: greater than 573 K for crystallization (Massalski *et al.*, 1986) and greater than 801 K for remorphization (Behera *et al.*, 2017). This highlights how thermal modulation is not limited to bonding transitions (as in GST), but can also be driven by well-engineered energetic asymmetries. These characteristics

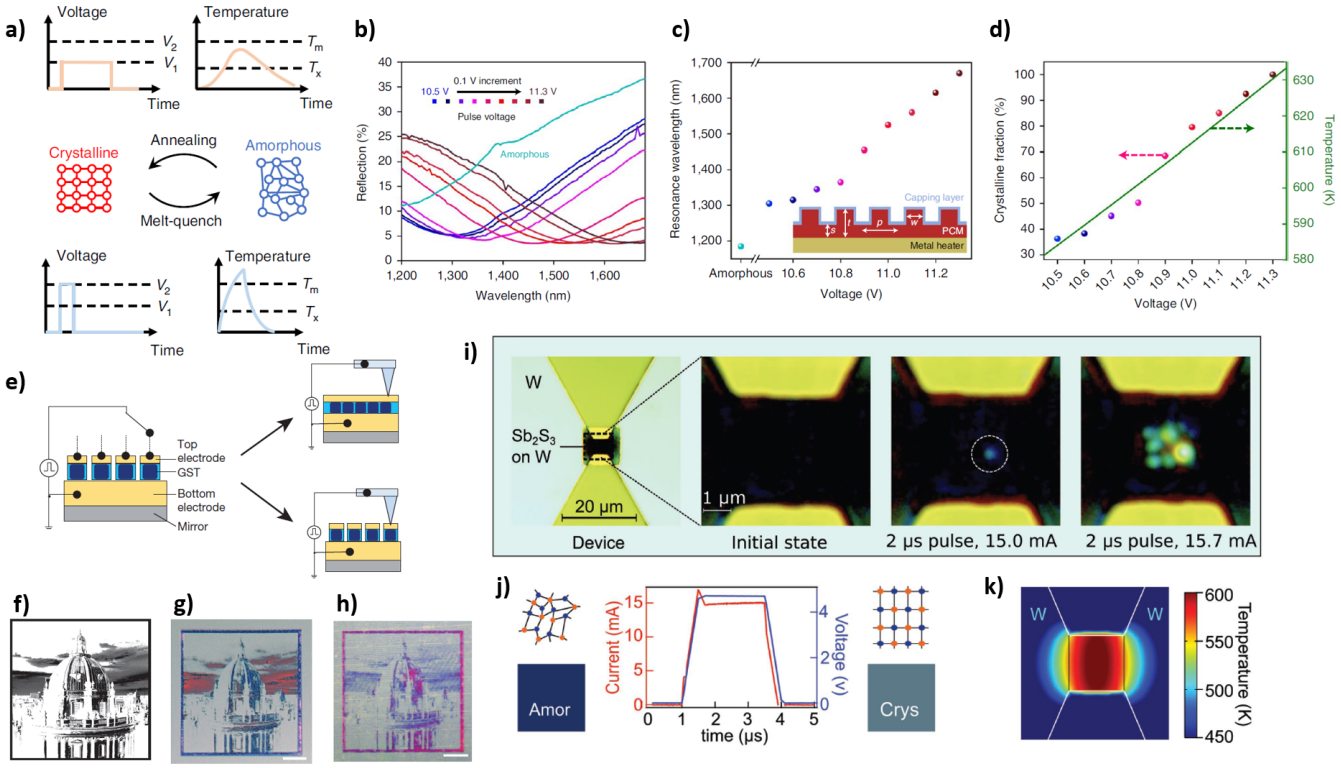

FIG. 3: **Representative demonstrations of electrical switching mechanisms in phase-change materials (PCMs). (a)** Schematic voltage and temperature pulse profiles used for inducing crystallization and amorphization in GSST-based metasurfaces via electrothermal control. The voltages V_1 and V_2 correspond to annealing and melt-quenching cycles, respectively. Adapted from (Zhang *et al.*, 2021) **(b-d)** Tunable optical response of a GSST metasurface as a function of pulse voltage: **(b)** reflection spectra under incremental voltage pulses (10.5-11.3 V), **(c)** corresponding redshift in resonance wavelength, and **(d)** extracted crystalline fraction vs. voltage showing continuous modulation. Adapted from (Zhang *et al.*, 2021), **(e-h)** Electrically induced image construction on a blanket ITO/GST/ITO/Pt stack using conductive AFM. **(e)** Schematic of the setup, **(f)** original grayscale image, **(g)** electrically written pattern after phase change, and **(h)** experimental pixel array reconstruction. Adapted from (Hosseini *et al.*, 2014). **(i-k)** Electrical switching of Sb_2S_3 using current pulses in a W/Sb_2S_3/W structure. **(i)** Device layout and optical images before and after switching with increasing current (15.0-15.7 mA), **(j)** pulse timing diagram and simulated structural states, and **(k)**finite element simulation of local Joule heating under applied bias. Adapted from (Dong *et al.*, 2019).

position Sb_2S_3 as a thermally stable, low-loss platform for nonvolatile and reconfigurable photonic systems.

B. Electrical Switching

Electrothermal switching provides a scalable and fully solid-state approach to electrically driven modulation in phase-change metasurfaces. Zhang *et al.* implemented this concept using a low loss chalcogenide alloy, GSST, structured into metaatoms atop reflective heaters. By applying tailored voltage pulses, crystallization is induced through long, low-voltage Joule heating, while short, high-voltage pulses trigger re-amorphization via melt-quenching (Fig. 3 a)) (Zhang *et al.*, 2021). By avoiding current flow directly through the PCM, this design ensures homogenous switching across large areas, essential for consistent multi-level tuning in optically thick films.

Figure 3 **b)** presents the reflectance spectra recorded after the crystallization pulses of increasing voltage; the resonance peak shifts to longer wavelengths as the fraction of crystallized volume in the GSST layer increases. The resonance shifts from 1190 to 1680 nm as the pulse voltage increases, indicating that the device supports incremental changes in optical response instead of discrete switching states. The resonance shift as a function of pulse voltage is presented in Figure 3 **c)**, while the extracted crystalline fraction versus the voltage derived by the Lorentz-Lorenz effective medium theory is shown in Figure 3 **d)** (Zhang *et al.*, 2021). The strong correlation between electrical input and optical output highlights the suitability of GSST for fine-tuned metasurface control,

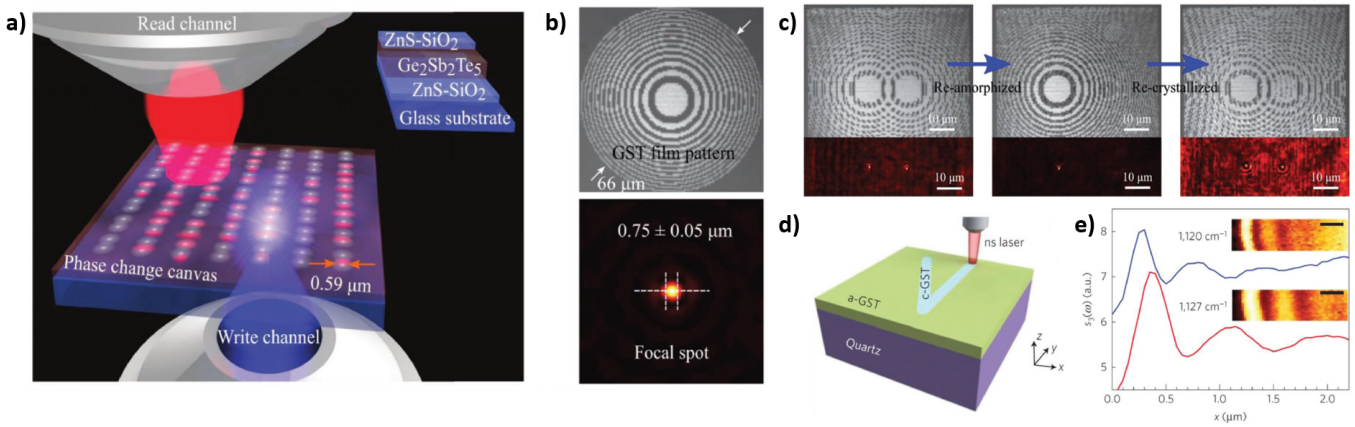

FIG. 4: **Optical switching mechanisms in phase-change materials. (a-c)** Laser-based optical writing, erasing, and re-writing of Fresnel zone-plate metasurfaces on GST films using a Ti:sapphire pulsed laser system. The focused laser pulses locally induce phase transitions between amorphous and crystalline states, enabling reversible and reconfigurable photonic patterns. **(d)** Schematic of laser-induced switching in a V-shaped GST region on quartz, illustrating directional phase conversion under nanoscale irradiation. **(e)** Optical phonon-polariton modes at 1120 and 1127 cm^{-1}, captured during laser-induced re-crystallization, further confirm the phase-dependent optical response at sub-diffraction scales. These demonstrations highlight the viability of contactless, high-resolution optical switching for non-volatile metasurface programming and structural color applications. Adapted from (Ding *et al.*, 2019), **(a–c)** adapted from (Wang *et al.*, 2016), and **(d-e)** adapted from (Li *et al.*, 2016).

with phase uniformity enabled by the optimized heater geometry established earlier.

Thin-film PCMs, particularly GST, have been widely studied in optical data storage, yet their integration into display and visualization systems has only recently gained momentum. Hosseini *et al.* pioneered an opto-electronic approach based on nanoscale electrical switching of GST integrated into multilayer reflective stacks. In their design, a GST film is sandwiched between transparent ITO electrodes and deposited on a reflective substrate Pt, forming a vertical architecture where localized crystallization modulates reflectivity through interference effects (Fig. 3 **e**). Using conductive AFM (CAFM), they demonstrated nanoscale patterning of arbitrary grayscale images, such as the Radcliffe Camera (Fig. 3 **f**)), by inducing controlled phase transitions in selected regions of the PCM. Electrical switching of the blanket film produced a clear visual contrast between the amorphous and crystalline areas, observable under standard optical microscopy without the need for image enhancement (Fig. 3 **g**)). This contrast closely matches that achieved in 300 nm x 300 nm lithographically defined pixel arrays (Fig. 3 **h**)), supporting the reliability of the continuous film switching approach and its applicability to high-resolution reconfigurable PCM-based displays.

Dong *et al.* demonstrated electrical switching of Sb_2S_3 by integrating it with tungsten filaments that act as resistive heaters. The configuration enables Joule heating upon current application, driving a phase transition without direct current flow through the PCM. Figure 3 **i)** shows optical images of the device before and after two successive current pulses (15.0 and 15.7 mA, 2 μs). As the current increases, a distinct region undergoes crystallization, which is reflected by a change in visible contrast. Figure 3 **j)** shows the current and voltage profiles used for pulse application, with schematic representations of the amorphous and crystalline phases. Finite element simulations of the heat distribution (Fig. 3 **k**)) confirm that the central region exceeds the crystallization threshold of Sb_2S_3, resulting in localized switching. Although effective, this design exhibits sensitivity to current overshoot, which can induce thermal ablation. However, it confirms that Sb_2S_3 allows fast reversible switching through electrically delivered thermal pulses in a metal-PCM-metal geometry (Dong *et al.*, 2019).

C. Optical Switching

Optical switching of phase-change materials enables localized, reversible control of optical properties using short, high-intensity laser pulses to induce crystallization or amorphization without physical contact. This mechanism is based on foundational concepts from optical data storage, where precise heating and quenching modulate the atomic structure of materials such as GST. As shown in Figure 4 **a-c**, Ding *et al.* (Ding *et al.*, 2019) demonstrated how femtosecond laser pulses can write, erase, and rewrite Fresnel zone plate metasurfaces in GST films. Devices such as lenses and grayscale holograms were reconfigured by modulating the number and energy of laser pulses, enabling diffraction-limited resolution with focal

spots below 1 µm.

This laser-driven mechanism eliminates the need for Joule heating or electrodes, offering spatial selectivity and high-speed operation compatible with all-dielectric platforms. Wuttig *et al.* (Wuttig *et al.*, 2017) highlighted how such optical patterning enables the creation of functional nanophotonic devices without lithography or metals, mitigating optical losses while allowing for pixel-level reconfiguration. Notably, Figure 4**d-e** presents results from Li *et al.* (Li *et al.*, 2016), showing the directional switching of the crystalline domains in an amorphous GST matrix and the corresponding shifts in mid-infrared phonon-polariton modes, further confirming the phase sensitivity of optically defined resonators.

Dong *et al.* (Dong *et al.*, 2019) extended this concept to Sb_2S_3, demonstrating reversible switching using nanosecond pulses, challenging its classification as a write-once material. Transitions were induced entirely by localized absorption, bypassing substrate heating, and allowing modulation at sub-100 ns timescales. This approach retains the low-loss character of Sb_2S_3 in the visible, supporting its use in reconfigurable color devices. Building on this, Yimam *et al.* (Yimam *et al.*, 2024) employed focused ion beam sculpting of Sb_2Se_3 to fine-tune reflectance across nanoscale domains, highlighting new opportunities to combine optical phase control with geometric structuring in display and metasurface technologies.

D. Outlook and Perspectives

Although thermal, electrical, and optical switching all enable phase transitions in PCMs, their operational regimes, device compatibility, and integration challenges differ significantly. Thermal switching, though conceptually simple and uniform across large areas, lacks spatial selectivity and is slow due to heating and cooling cycle constraints. Its value lies in experimental accessibility and scalability for planar architectures, but it is less suited to applications demanding local control or fast modulation.

Electrical switching offers compact integration with voltage-driven architectures, allowing reversible transitions via Joule heating or conductive AFM. As demonstrated by Zhang *et al.* and Hosseini *et al.*, electrothermal and nanoscale switching methods unlock multilevel reflectance tuning and pixel-addressability without requiring optical alignment. However, direct contact and heat dissipation challenges persist, especially in dense arrays. Device reliability is sensitive to electrode design, and amorphization requires precise pulse engineering to avoid thermal overshoot.

In contrast, optical switching uniquely combines non-contact operation with sub-micrometer precision. The work of Ding *et al.*, Wuttig *et al.*, and Dong *et al.* demonstrates that laser pulses enable reversible patterning of PCMs with high spatial resolution, enabling devices such as grayscale holograms, metasurface lenses, and polaritonic resonators. This approach avoids metal-induced losses, supports fast switching, and directly benefits from advances in optical storage technologies. However, its scalability to large-area applications and integration with electronics remain less developed.

A compelling direction emerges from Yimam *et al.*, who demonstrate that focused ion beam (FIB) nanostructuring of Sb_2Se_3 films offers spatial control and reflectance tuning at resolutions beyond the diffraction limit. Although FIB does not involve thermal or photonic excitation, the resulting local changes in thickness and structure mimic the optical contrast achievable through laser writing. This blurs the distinction between geometric and phase-based modulation, suggesting hybrid strategies in which material reconfiguration and physical structuring co-engineer the optical response.

Overall, future development of reconfigurable photonics will likely benefit from hybrid switching platforms that combine the scalability of thermal activation, the integration potential of electrical control, and the spatial precision of optical methods. Materials such as Sb_2S_3 and Sb_2Se_3, with wide band gaps and low absorption in the visible, offer a promising foundation for these approaches. Efforts to expand endurance, reduce energy consumption, and develop addressable architectures will be critical to advancing PCMs toward programmable optical metasurfaces, structural color displays, and rewritable nanophotonic components.

IV. APPLICATIONS IN NANOPHOTONICS AND OPTOELECTRONICS

The pronounced and reversible changes in refractive index and absorption across phase states in PCMs have opened new pathways for dynamic optical devices. Among the most promising applications is the generation of tunable structural color, where phase transitions can actively modulate the interference-driven coloration of nanostructured surfaces. This capability enables a shift from static optical components toward reconfigurable photonic elements, such as metasurfaces and display pixels, with optical responses that can be updated post-fabrication. Early demonstrations by Hosseini et al. showed that ultrathin GST films embedded within ITO-based multilayers could act as electrically reconfigurable reflectors. As discussed in Section II, these films were used to render complex microimages, including university logos and building facades, with high optical contrast and a sub-10 μ m pixel definition. Although not reprinted here, these experiments remain pivotal in demonstrating that PCM-based reflectors can reach display-level resolution using purely electronic switching without mechan-

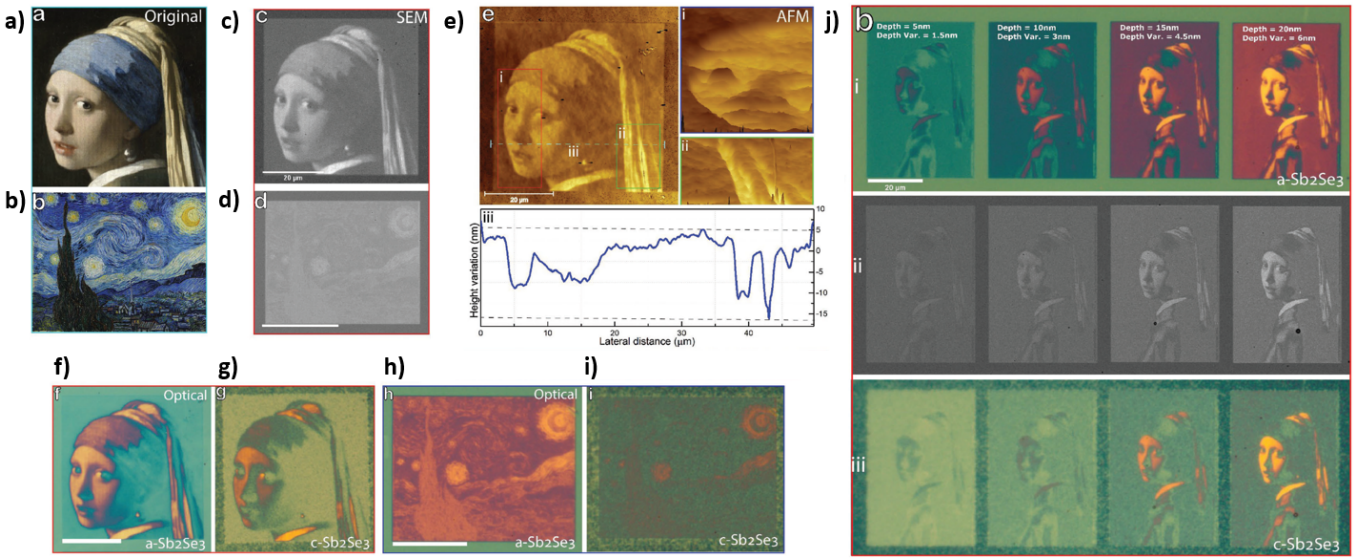

FIG. 5: **High-resolution structural color generation using 3D nanopatterned Sb_2Se_3 thin films. a-b)** Grayscale images of "Girl with a Pearl Earring" and "Starry Night" used as digital templates for nanopatterning. **c-d)** SEM images of the Sb_2Se_3 metastructures after focused ion beam (FIB) milling on reflective substrates. **e)** Atomic force microscopy (AFM) scan of the printed surface, showing nanoscale height variations with lateral resolution below 50 nm; subpanels **(i-iii)** illustrate fine surface features and extracted height profiles. **(f-g)** Optical micrographs of the fabricated metasurfaces in the amorphous phase. **(h-i)** Corresponding optical images after crystallization, showing clear phase-dependent contrast and coloration. **j)** Structural color rendering based on FIB-controlled milling depth: **i** contrast states generated by varying depth from 5 to 20 nm; **ii** corresponding BSE-SEM image showing depth-dependent contrast; **iii** crystallization-induced additional contrast state. Together, these demonstrate grayscale and spectral tuning through geometric and phase control in Sb_2Se_3 films. Figure adapted from Figures 4 and 5 in (Yimam *et al.*, 2024).

ical parts. Recent advances have expanded these capabilities using widebandgap PCMs with lower optical loss, such as Sb_2Se_3. In particular, Yimam et al. introduced a novel fabrication approach that combines focused ion beam (FIB) milling with thin film Sb2Se3 to achieve reconfigurable ultrahigh-resolution structural color. Figure X presents this concept. The grayscale digital artworks were nanoprinted onto thin films of Sb_2Se_3 deposited on reflective gold substrates **a-b)**. The corresponding nanostructures revealed through SEM **c-d)** and AFM **e)** profiling demonstrate controlled surface relief over tens of nanometers in height. This nanoscale topography directly modulates visible reflectance.

The panels **f-i)** show the printed structures in amorphous and crystalline forms. The change in phase causes visible differences in hue and brightness in the same regions. The colors deepen or shift in some areas while others gain contrast, making the effect perceptible without magnification. Finally, panel **j)** illustrates grayscale contrast generation by controlling the local grinding depth and lateral dimensions. The subpanels **i)-iii)** demonstrate how geometric tuning and crystallization can be used independently or jointly to modulate reflection and contrast. Together, these results demonstrate that 3D nanostructuring of Sb_2Se_3 enables dynamic, reprogrammable color control with diffraction-limited resolution without relying on lossy metals or organic emitters.

A. Outlook and Perspectives

Although recent demonstrations have pushed structural color resolution to the diffraction limit using FIB-patterned Sb_2Se_3 films (Yimam *et al.*, 2024), several challenges remain. Focused ion beam milling, though precise, is inherently slow and unsuitable for large-area or scalable manufacturing. Moreover, while phase-change modulation offers high contrast, current demonstrations lack electrically addressable architectures at the nanoscale. Earlier approaches using multilayer stacks and electrical switching (Hosseini *et al.*, 2014) remain more compatible with integration, but suffer from absorption losses and limited spatial tunability. Bridging these approaches, combining high-resolution patterning with fast localized switching, will be essential to advance dynamic PCM-based displays and metasurfaces. Furthermore, the long-term cycling stability, endurance and environmental robustness of wideband-gap PCMs like Sb_2Se_3 require further investigation before deployment in practical reconfigurable photonic systems.

V. CONCLUSIONS

Phase-change materials provide a compelling platform for reconfigurable photonics, especially in the context of structural color generation in the visible spectrum. This review has examined how the strong contrast in refractive index and absorption between phase states enables dynamic tuning of optical responses and how this tunability can be exploited through thermal, electrical, and optical switching mechanisms. Among the materials surveyed, wide-band-gap chalcogenides such as Sb_2S_3 and Sb_2Se_3 offer promising optical performance with minimal losses in the visible range, expanding the design space beyond traditional PCM systems such as GST and VO_2.

Practical demonstrations, including electrically programmable metasurfaces and FIB-fabricated nanoprints, illustrate the potential for subwavelength-resolution structural color with dual-phase functionality. However, challenges remain in scaling fabrication methods, achieving fast and addressable switching, and improving long-term endurance and environmental stability. Future advances will depend on the integration of nanoscale patterning techniques with efficient switching architectures and on further material innovation to balance optical performance, reliability, and manufacturability.

VI. BIBLIOGRAPHY

REFERENCES

Abdollahramezani, Sajjad, Omid Hemmatyar, Hossein Taghinejad, Alex Krasnok, Yashar Kiarashinejad, Mohammadreza Zandehshahvar, Andrea Alù, and Ali Adibi (2020), en"Tunable nanophotonics enabled by chalcogenide phase-change materials," Nanophotonics **9** (5), 1189–1241.

Arun, P, and A. G. Vedeshwar (1997), "Effect of heat treatment on the optical properties of amorphous Sb2S3 film: The possibility of optical storage," Journal of Non-Crystalline Solids **220** (1), 63–68.

Behera, Jitendra K, Xilin Zhou, Junji Tominaga, and Robert E. Simpson (2017), EN"Laser switching and characterisation of chalcogenides: systems, measurements, and applicability to photonics [Invited]," Optical Materials Express **7** (10), 3741–3759.

Burkhard, George F, Eric T. Hoke, and Michael D. McGehee (2010), "Accounting for Interference, Scattering, and Electrode Absorption to Make Accurate Internal Quantum Efficiency Measurements in Organic and Other Thin Solar Cells," Advanced Materials **22** (30), 3293–3297.

Cao, Tun, and Mengjia Cen (2019), en"Fundamentals and Applications of Chalcogenide Phase-Change Material Photonics," Advanced Theory and Simulations **2** (8), 1900094.

Carrillo, Santiago García-Cuevas, Liam Trimby, Yat-Yin Au, V. Karthik Nagareddy, Gerardo Rodriguez-Hernandez, Peiman Hosseini, Carlos Ríos, Harish Bhaskaran, and C. David Wright (2019), en"A Nonvolatile Phase-Change Metamaterial Color Display," Advanced Optical Materials **7** (18), 1801782.

Cheng, Zengguang, Tara Milne, Patrick Salter, Judy S. Kim, Samuel Humphrey, Martin Booth, and Harish Bhaskaran (2021), "Antimony thin films demonstrate programmable optical nonlinearity," Science Advances **7** (1), eabd7097.

Ding, Fei, Yuanqing Yang, and Sergey I. Bozhevolnyi (2019), en"Dynamic Metasurfaces Using Phase-Change Chalcogenides," Advanced Optical Materials **7** (14), 1801709.

Dirac, Paul Adrien Maurice, and Niels Henrik David Bohr (1927), "The quantum theory of the emission and absorption of radiation," Proceedings of the Royal Society of London. Series A, Containing Papers of a Mathematical and Physical Character **114** (767), 243–265.

Dong, Weiling, Hailong Liu, Jitendra K. Behera, Li Lu, Ray J. H. Ng, Kandammathe Valiyaveedu Sreekanth, Xilin Zhou, Joel K. W. Yang, and Robert E. Simpson (2019), en"Wide Bandgap Phase Change Material Tuned Visible Photonics," Advanced Functional Materials **29** (6), 1806181.

Fang, Xinyuan, Haoran Ren, and Min Gu (2020), en"Orbital angular momentum holography for high-security encryption," Nature Photonics **14** (2), 102–108.

Fermi, Enrico (1932), "Quantum Theory of Radiation," Reviews of Modern Physics **4** (1), 87–132.

Feynman, Richard P (1960), en"There's Plenty of Room at the Bottom," Engineering and Science **23** (5), 22–36.

Freestone, Ian, Nigel Meeks, Margaret Sax, and Catherine Higgitt (2007), en"The Lycurgus Cup — A Roman nanotechnology," Gold Bulletin **40** (4), 270–277.

Gabor, Dennis (1972), "Holography, 1948-1971," Science **177** (4046), 299–313.

Gholipour, Behrad, Artemios Karvounis, Jun Yin, Cesare Soci, Kevin F. MacDonald, and Nikolay I. Zheludev (2018), en"Phase-change-driven dielectric-plasmonic transitions in chalcogenide metasurfaces," NPG Asia Materials **10** (6), 533–539.

Ghosh, C, and B. P. Varma (1979), "Optical properties of amorphous and crystalline Sb2S3 thin films," Thin Solid Films **60** (1), 61–65.

Hafermann, Martin, Philipp Schöppe, Jura Rensberg, and Carsten Ronning (2018), "Metasurfaces Enabled by Locally Tailoring Disorder in Phase-Change Materials," ACS Photonics **5** (12), 5103–5109.

Han, Song, Longqing Cong, Yogesh Kumar Srivastava, Bo Qiang, Mikhail V. Rybin, Abhishek Kumar, Ravikumar Jain, Wen Xiang Lim, Venu Gopal Achanta, Shriganesh S. Prabhu, Qi Jie Wang, Yuri S. Kivshar, and Ranjan Singh (2019), en"All-Dielectric Active Terahertz Photonics Driven by Bound States in the Continuum," Advanced Materials **31** (37), 1901921.

Hosseini, Peiman, C. David Wright, and Harish Bhaskaran (2014), en"An optoelectronic framework enabled by low-dimensional phase-change films," Nature **511** (7508), 206–211.

Kats, Mikhail A, Romain Blanchard, Patrice Genevet, and Federico Capasso (2013), en"Nanometre optical coatings based on strong interference effects in highly absorbing media," Nature Materials **12** (1), 20–24.

Ko, Joo Hwan, Young Jin Yoo, Yubin Lee, Hyeon-Ho Jeong, and Young Min Song (2022), "A review of tunable photonics: Optically active materials and applications from visible to terahertz," iScience **25** (8), 104727.

Kolobov, A V, P. Fons, J. Tominaga, A. L. Ankudinov, S. N. Yannopoulos, and K. S. Andrikopoulos (2004), en"Crystallization-induced short-range order changes in amorphous GeTe," Journal of Physics: Condensed Matter

16 (44), S5103.
Lee, Bong-Sub, John R. Abelson, Stephen G. Bishop, Dae-Hwan Kang, Byung-ki Cheong, and Ki-Bum Kim (2005), en"Investigation of the optical and electronic properties of Ge2Sb2Te5 phase change material in its amorphous, cubic, and hexagonal phases," Journal of Applied Physics **97** (9), 093509.
Lencer, Dominic, Martin Salinga, Blazej Grabowski, Tilmann Hickel, Jörg Neugebauer, and Matthias Wuttig (2008), en"A map for phase-change materials," Nature Materials **7** (12), 972–977.
Li, Peining, Xiaosheng Yang, Tobias W. W. Maß, Julian Hanss, Martin Lewin, Ann-Katrin U. Michel, Matthias Wuttig, and Thomas Taubner (2016), eng"Reversible optical switching of highly confined phonon-polaritons with an ultrathin phase-change material," Nature Materials **15** (8), 870–875.
Liu, Hailong, Weiling Dong, Hao Wang, Li Lu, Qifeng Ruan, You Sin Tan, Robert E. Simpson, and Joel K. W. Yang (2020), "Rewritable color nanoprints in antimony trisulfide films," Science Advances **6** (51), eabb7171.
Lu, Li, Weiling Dong, Jitendra K. Behera, Litian Chew, and Robert E. Simpson (2019), en"Inter-diffusion of plasmonic metals and phase change materials," Journal of Materials Science **54** (4), 2814–2823.
Lucovsky, G, and R. M. White (1973), en"Effects of Resonance Bonding on the Properties of Crystalline and Amorphous Semiconductors," Physical Review B **8** (2), 660–667.
Massalski, Thaddeus B, Hiroaki Okamoto, PRnbsp Subramanian, Linda Kacprzak, and William W. Scott (1986), *Binary alloy phase diagrams*, Vol. 1 (American society for metals Metals Park, OH).
Michel, Ann-Katrin U, Matthias Wuttig, and Thomas Taubner (2017), en"Design Parameters for Phase-Change Materials for Nanostructure Resonance Tuning," Advanced Optical Materials **5** (18), 1700261.
Nassau, Kurt (1987), en"The fifteen causes of color: The physics and chemistry of color," Color Research & Application **12** (1), 4–26.
Ozbay, Ekmel (2006), "Plasmonics: Merging Photonics and Electronics at Nanoscale Dimensions," Science **311** (5758), 189–193.
Raeis-Hosseini, Niloufar, and Junsuk Rho (2017), en"Metasurfaces Based on Phase-Change Material as a Reconfigurable Platform for Multifunctional Devices," Materials **10** (9), 1046.
Raoux, Simone, Feng Xiong, Matthias Wuttig, and Eric Pop (2014), en"Phase change materials and phase change memory," MRS Bulletin **39** (8), 703–710.
Ren, Haoran, Xinyuan Fang, Jaehyuck Jang, Johannes Bürger, Junsuk Rho, and Stefan A. Maier (2020), en"Complex-amplitude metasurface-based orbital angular momentum holography in momentum space," Nature Nanotechnology **15** (11), 948–955.
Rivera, Nicholas, and Ido Kaminer (2020), en"Light–matter interactions with photonic quasiparticles," Nature Reviews Physics **2** (10), 538–561.
Ríos, Carlos, Peiman Hosseini, Robert A. Taylor, and Harish Bhaskaran (2016), "Color Depth Modulation and Resolution in Phase-Change Material Nanodisplays," Advanced Materials **28** (23), 4720–4726.
Selvaraja, Shankar Kumar, Purnima Sethi, Shankar Kumar Selvaraja, and Purnima Sethi (2018), en"Review on Optical Waveguides," in en*Emerging Waveguide Technology* (IntechOpen).
Shportko, Kostiantyn, Stephan Kremers, Michael Woda, Dominic Lencer, John Robertson, and Matthias Wuttig (2008), en"Resonant bonding in crystalline phase-change materials," Nature Materials **7** (8), 653–658.
Sreekanth, Kandammathe Valiyaveedu, Rohit Medwal, Yogesh Kumar Srivastava, Manukumara Manjappa, Rajdeep Singh Rawat, and Ranjan Singh (2021), "Dynamic Color Generation with Electrically Tunable Thin Film Optical Coatings," Nano Letters **21** (23), 10070–10075.
Sun, Xinxing, Andriy Lotnyk, Martin Ehrhardt, Jürgen W. Gerlach, and Bernd Rauschenbach (2017), en"Realization of Multilevel States in Phase-Change Thin Films by Fast Laser Pulse Irradiation," Advanced Optical Materials **5** (12), 1700169.
Tominaga, Junji, Takayuku Shima, Paul Fons, Robert Simpson, Masashi Kuwahara, and Alexander Kolobov (2009), en"What is the Origin of Activation Energy in Phase-Change Film?" Japanese Journal of Applied Physics **48** (3S1), 03A053, publisher: IOP Publishing.
Wang, Kangpeng, Raphael Dahan, Michael Shentcis, Yaron Kauffmann, Adi Ben Hayun, Ori Reinhardt, Shai Tsesses, and Ido Kaminer (2020), en"Coherent interaction between free electrons and a photonic cavity," Nature **582** (7810), 50–54.
Wang, Qian, Edward T. F. Rogers, Behrad Gholipour, Chih-Ming Wang, Guanghui Yuan, Jinghua Teng, and Nikolay I. Zheludev (2016), en"Optically reconfigurable metasurfaces and photonic devices based on phase change materials," Nature Photonics **10** (1), 60–65, publisher: Nature Publishing Group.
Wuttig, M, H. Bhaskaran, and T. Taubner (2017), en"Phase-change materials for non-volatile photonic applications," Nature Photonics **11** (8), 465–476.
Wuttig, Matthias, and Noboru Yamada (2007), en"Phase-change materials for rewriteable data storage," Nature Materials **6** (11), 824–832.
Yamada, Noboru, Eiji Ohno, Nobuo Akahira, Ken'ichi Nishiuchi, Ken'ichi Nagata, and Masatoshi Takao (1987), en"High Speed Overwritable Phase Change Optical Disk Material," Japanese Journal of Applied Physics **26** (S4), 61.
Yimam, Daniel T, Minpeng Liang, Jianting Ye, and Bart J. Kooi (2024), en"3D Nanostructuring of Phase-Change Materials Using Focused Ion Beam toward Versatile Optoelectronics Applications," Advanced Materials **36** (23), 2303502.
Yu, Cunjiang, Yuhang Li, Xun Zhang, Xian Huang, Viktor Malyarchuk, Shuodao Wang, Yan Shi, Li Gao, Yewang Su, Yihui Zhang, Hangxun Xu, Roger T. Hanlon, Yonggang Huang, and John A. Rogers (2014), "Adaptive optoelectronic camouflage systems with designs inspired by cephalopod skins," Proceedings of the National Academy of Sciences **111** (36), 12998–13003.
Zhang, Yifei, Jeffrey B. Chou, Junying Li, Huashan Li, Qingyang Du, Anupama Yadav, Si Zhou, Mikhail Y. Shalaginov, Zhuoran Fang, Huikai Zhong, Christopher Roberts, Paul Robinson, Bridget Bohlin, Carlos Ríos, Hongtao Lin, Myungkoo Kang, Tian Gu, Jamie Warner, Vladimir Liberman, Kathleen Richardson, and Juejun Hu (2019), en"Broadband transparent optical phase change materials for high-performance nonvolatile photonics," Nature Communications **10** (1), 4279.
Zhang, Yifei, Clayton Fowler, Junhao Liang, Bilal Azhar,

Mikhail Y. Shalaginov, Skylar Deckoff-Jones, Sensong An, Jeffrey B. Chou, Christopher M. Roberts, Vladimir Liberman, Myungkoo Kang, Carlos Ríos, Kathleen A. Richardson, Clara Rivero-Baleine, Tian Gu, Hualiang Zhang, and Juejun Hu (2021), en"Electrically reconfigurable non-volatile metasurface using low-loss optical phase-change material," Nature Nanotechnology **16** (6), 661–666.

Zhu, Min, Oana Cojocaru-Mirédin, Antonio M. Mio, Jens Keutgen, Michael Küpers, Yuan Yu, Ju-Young Cho, Richard Dronskowski, and Matthias Wuttig (2018), eng"Unique Bond Breaking in Crystalline Phase Change Materials and the Quest for Metavalent Bonding," Advanced Materials (Deerfield Beach, Fla.) **30** (18), e1706735.